Origin of Knudsen forces on heated microbeams

Taishan Zhu[1] and Wenjing Ye[1,2]
[1]*Department of Mechanical Engineering, The Hong Kong University of Science and Technology, Clear Water Bay, Kowloon, Hong Kong*
[2]*KAUST-HKUST Micro/Nanofluidic Joint Laboratory, The Hong Kong University of Science and Technology, Clear Water Bay, Kowloon, Hong Kong*
(Received 23 March 2010; published 9 September 2010)

The presented work probes the fundamentals of Knudsen forces. Using the direct simulation Monte Carlo (DSMC) method, the flows induced by temperature inhomogeneity within a representative configuration and the Knudsen force acting on a heated microbeam are captured as functions of Knudsen number in the entire flow regime. Both flow strength and Knudsen force peak in the transition regime and negative Knudsen force absent in experimental data is observed. The mechanisms of the thermally induced flows and Knudsen forces are studied. It has been found that thermal edge flow is the main driven source for the formation of the Knudsen force on microbeams and domain configuration plays an important role in the process.

DOI: 10.1103/PhysRevE.82.036308 PACS number(s): 47.61.Fg, 51.10.+y, 85.85.+j

I. INTRODUCTION

Interests in thermal actuation driven by rarefied gas have recently revived in the field of micro-/nanoelectromechanical systems (MEMS/NEMS), largely due to its promising applications and its feasibility demonstrated by the experimental and analytical works by Passion *et al.* [1–3], Gotsmann *et al.* [4], Scandurra *et al.* [5], Selden *et al.* [6] and others. The well known radiometer utilizing radiometric forces arising in a low-pressure ambient is perhaps the first application, of which the history can be traced back to early experiments conducted by Abraham Bennet in 1792, Fresnel in 1825, as well as those in 1870s by Crooks [7] and Reynolds [8]. The fundamental analyses by Maxwell [9] and Knudsen [10], and the later theory by Einstein in 1909 [11], together with recent experimental and numerical studies by Carbone, *et al.* [12], Selden, *et al.* [6] have made radiometric forces less mysterious. Conceptual applications based on these forces have been proposed, for example, radiometric propulsion system [13], microactuator [14] and mesosphere flight vehicle [15,16].

Less well known but equally intriguing is the thermal force acting on an object with uniform temperature placed in a rarefied gas with a nonuniform temperature field [1–4]. Although such a mechanical force, denoted as the Knudsen force in this paper, is often negligible in both continuum and free-molecule regimes, there exist scenarios where it is observable and significant particularly in miniature devices, among which the atomic force microscopes and Pirani gauges are cases in point. Such a mechanical effect might probably, on the one hand, deteriorate the performance of those MEMS devices; on the other hand, it may well be exploited as energy sources for novel applications. It is worth pointing out that there exist other types of Knudsen forces arising from temperature gradients. In fact, the radiometric force is one of them. In the present study, only the force acting on a structure with uniform temperature is of interest.

In high vacuum situations, theoretical analysis can be conducted based on gas kinetic theory. Passian *et al.* [1] derived the expression of Knudsen force on a heated cantilever next to a substrate inside a vacuum enclosure, and it reads

$$F = \frac{p_r}{2}\left[\sqrt{\frac{a_s\tau_s + a_{cb}(1-a_s)\tau_c}{a_s + a_{cb} - a_s a_{cb}}} + \sqrt{\frac{a_{cb}\tau_c + a_s(1-a_{cb})\tau_s}{a_s + a_{cb} - a_s a_{cb}}} - \sqrt{1 - a_{ct} + a_{ct}\tau_c} - 1\right],$$

where the subscripts s, c, cb, ct denote the substrate, cantilever, cantilever bottom and cantilever top, respectively; a_i, $i=s,cb,ct$ signify the corresponding accommodation coefficients; $\tau_j = T_j/T_r$ $(j=s,c,cb,ct)$ and T_r, p_r are the temperature and pressure of the ambient. It should be noted that there is a minor typo in the original formula presented in [1]. The sign of the last term should be minus instead of plus. With this correction, the formula predicts zero force, as expected, for the cases of fully diffuse walls and $\tau_s = 1$. In a later paper by Gotsman and Durig [4], Passian's formula was generalized for the prediction of the Knudsen force on a similar setup but operated in an open air. An empirical parameter, q, was introduced to account for the thermalization of gas molecules due to intermolecular collisions. The limit of $q=1$ corresponds to the free-molecule regime. In addition, another empirical parameter, A_{eff}, was used to represent the effective area. In both work, the Knudsen force is attributed primarily to partially accommodated walls and the difference in the accommodation coefficients. The edge effect is ignored because the cantilever was modeled as an infinite beam. In this paper, it is demonstrated that the edge of the beam plays an important role in the production of the Knudsen force.

For cases where intermolecular collisions are of comparable importance in gas transport, theoretical analysis is difficulty, if not impossible, to conduct. Passian *et al.* [3] conducted a series of experiments and observed that the Knudsen force was proportional to the ambient pressure in the low-pressure range, but inversely proportional to the pressure in the high-pressure range. The maximum force occurred in the transition regime. For Ar, the Knudsen force peaked at $\mathrm{Kn} \approx 0.6$. An empirical formula for collisional Knudsen forces was then obtained by fitting the detected signal $S(p) = (ap^{\alpha} + bp^{-\beta})^{-1}$. This form is very similar to the form, $F(p) = (ap^1 + bp^{-1})^{-1}$, proposed by Bruche and Littwin

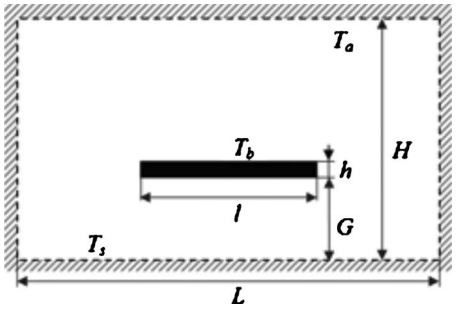

FIG. 1. Schematic illustration of the model problem.

for the prediction of radiometric forces [17]. The parameters in the formula, α and β, depend on not only gas properties but also on the geometric information of the device. Aleexeenko *et al.* simulated the Knudsen force on a heated microbeam next to a cold substrate for a wide range of Knudsen number. The ellipsoidal statistical (ES) kinetic model equation, an approximation of the Boltzmann equation, was employed and numerically solved. A qualitatively similar trend was obtained and it was found that the maximum force occurred at about $\mathrm{Kn} \approx 2.0$ [18].

Despite a few attempts on the modeling of the Knudsen force, a detailed and accurate analysis of the Knudsen force in the entire flow regime is yet to come. Moreover, the fundamentals and the origin of the Knudsen force are still elusive and have been seldom studied in the previous literature. In this paper a systematic study of the Knudsen force by means of the direct simulation Monte Carlo (DSMC) method [19] is presented. Of particular interest in this study is the gas flows induced by temperature gradients and the important role they play in the formation of the Knudsen force.

II. FORMULATION AND METHODOLOGY

Heated beams due to Joule and/or optical heating are commonly employed in microscale and nanoscale devices. Often they are placed next to a substrate and/or operated inside a vacuum enclosure. As depicted in Fig. 1, the two-dimensional (2D) model problem employed in this study consists of a hot rectangular beam with a thickness of h and a width of l, which is encompassed by a rectangular enclosure with a width of L and a height of H. The beam is placed at a fixed distance, G, away from the bottom wall of the enclosure which represents the substrate. The temperatures of the beam and the substrate are denoted as T_b and T_s, respectively. The top and the side walls of the enclosure are assumed to have the same temperature denoted as T_a. In some applications such as topographical sensing, the gap between the hot structure and the wall immediately beneath it, which represents the surface to be scanned, is often at the submicron scale. Hence the rarefaction of gas inside the enclosure could be caused by low pressure and/or by small scale.

When the temperature of the beam, T_b, is different from T_s and T_a, the vertical linear momentum fluxes imparted to the top and bottom surfaces of the beam are unbalanced, which gives rise to a net force, the Knudsen force, along the same direction. Denoting the vertical direction as the jth direction, the net normal force per unit area exerted by the impinging and outgoing molecules can be formulated as

$$p_j = mn \int_{-\infty}^{+\infty} \mathrm{d}c_i \int_{-\infty}^{+\infty} \mathrm{d}c_k \int_{-\infty}^{+\infty} \mathrm{d}c_j c_j^2 f(\mathbf{c}), \tag{1}$$

where m and n are molecular mass and number density, $\mathbf{c}$ denotes the molecular velocity with its three Cartesian components expressed as c_i, c_j, c_k, $f(\mathbf{c})$ is the velocity distribution function. It should be emphasized that the Knudsen force should not be calculated simply by taking the difference of the scalar pressures at the top and bottom surfaces of the beam, since only when the solid surface retains complete equilibrium with the host gas can the pressure tensor be isotropic and thereby the net force be calculated from the difference of the scalar pressure as in the classical gas dynamics [9]. To be specific, the diagonal terms of pressure tensor differentiate each other in nonequilibrium situations, thus the force should be calculated as $F = \oint_{\partial\Omega_c} \mathbf{n}\cdot\mathbf{P}\cdot\mathbf{n}\mathrm{d}s$ rather than $F = \frac{1}{3}\oint_{\partial\Omega_c} \mathbf{I}:\mathbf{P}\mathrm{d}s$, where $\mathbf{n}$ denotes the outward unit normal vector of the beam surfaces and $\mathbf{I}:\mathbf{P}$ is the trace of the pressure tensor which defines the thermodynamic pressure.

If the velocity distribution function is given, the Knudsen force can be readily calculated using expression (1). The Boltzmann equation provides a theoretical foundation for the solution of the distribution function for gases with arbitrary Knudsen number [19,20]. It reads

$$\frac{\partial}{\partial t}(nf) + \mathbf{c}\cdot\frac{\partial}{\partial \mathbf{r}}(nf) + \mathbf{F}\cdot\frac{\partial}{\partial \mathbf{c}}(nf) = Q, \tag{2}$$

where $Q = \int_{-\infty}^{\infty}\int_0^{4\pi} n^2(f^* f_1^* - f f_1) g \sigma \mathrm{d}\Omega \mathrm{d}^3 c_1$ is the collision integral which describes the change in the velocity distribution function due to intermolecular collisions. The complexity of the collision integral, however, renders theoretical analysis and numerical solution relatively formidable. As a result, simplifications to the original collision term have been proposed. Among various models, Bhatnagar-Gross-Krook (BGK) and ellipsoidal statistical (ES) models are most frequently applied in which a nonlinear relaxation term is employed instead of the full collision integral Q.

When the gas departs significantly from its equilibrium state, direct physical simulation approaches, such as molecular dynamics (MD) and the direct simulation Monte Carlo (DSMC) techniques, are more advantageous because of their high accuracy [19,21]. For problems of nonequilibrium gas transport, the DSMC has been well tested and employed for a wide range of Knudsen number [22]. Unlike molecular dynamic simulation, DSMC tracks a large number of simulated particles, each being a statistical representation of a large cluster of real molecules. The molecular motions and intermolecular collisions are decoupled over a small time interval. Particles undergo a free convection step followed by a collision step. The convection is treated deterministically while the intermolecular collisions are treated statistically. For a detailed description of the DSMC, readers are referred to [19]. In these types of particle methods, macroscopic quantities are obtained by averaging the corresponding microscopic quantities. Taking the Knudsen force for example,

it can be obtained from the net moment flux as

$$F_j = \sum_{\partial\Omega_c} p_j \mathrm{d}s = \frac{W_p}{m} \sum_{\partial\Omega_c} \langle M_j \cdot \dot{N}(M_j) \rangle \mathrm{d}s, \tag{3}$$

where W_p is the ratio of the mass of a simulated particle to that of a physical molecule, and $\dot{N}(M_j)$ is the number flux of molecules which transfer a net normal momentum M_j to the beam surface element $\mathrm{d}s$, $\partial\Omega_c$ represents the total beam surface contributing to the Knudsen force. The averaging operator in Eq. (3) denotes the ensemble averaging for unsteady problems and the time averaging for steady cases. In the model problem, time averaging is employed.

III. RESULTS AND ANALYSES

A. Temperature field and Knudsen force

DSMC simulations are carried out on a grid with its cell size, l_c, determined based on the criteria of $l_c = \min(G/10, \lambda/3)$ and with a time step as $\tau = \alpha l_c (2RT_{\max})^{-1/2}$, where λ is the mean free path of gas molecules, α is a value less than unit, R is the gas constant and $T_{\max}$ is the maximum temperature within the domain. Argon is filled between the beam and the chamber, of which the temperatures are 500 and 300 K, respectively. Variable hard sphere molecules and Maxwell gas-surface interaction model are employed. All walls are assumed to be fully diffuse. A series of simulations with different chamber and beam dimensions have been performed, and the temperature fields of cases with 20×8 $\mu\mathrm{m}^2$ chamber and 10×2 $\mu\mathrm{m}^2$ beam at three different Knudsen numbers are presented in Fig. 2, representing the near continuum, transition and free-molecule regimes. These Knudsen numbers are calculated based on the average temperature of the beam and the chamber and the gap G. Due to symmetry, only the right half of the domain is shown. The temperature contours change significantly from the slightly rarefied (Kn=0.056) case to the highly rarefied case (Kn=56) in which noticeable kinks in the contour lines are observed. These kinks are originated at the sharp corners of the beam. Unlike the slightly rarefied cases in which intermolecular collisions quickly smooth out those kinks near the corners, the lack of sufficient intermolecular collisions in the highly rarefied cases allows these kinks to propagate much further away from the corners as shown in Fig. 2(c).

Knudsen forces per unit length at various Knudsen numbers are calculated and plotted in Fig. 3, indicated by dots. The solid curve is the fitting line based on the simulation data. Due to the statistical noise, large fluctuations are observed in the calculated Knudsen forces in the range of Kn <0.2. The direction and the general trend of the simulated Knudsen force are qualitatively consistent with the measured data within a large range of the Knudsen number [3], i.e., the force is inversely proportional to the Knudsen number in the low-pressure range and proportional to the Knudsen number in the high-pressure range. The maxima of the Knudsen force occurs between Kn=0.3 and Kn=0.4, which is not too far from 0.6, the measured data in Passian *et al.*'s experiment.

Another important feature in the simulated Knudsen force is the reverse in its direction near Kn=1. From Kn=1.5 to Kn=30, the direction of the force is pointing toward the gap instead of pointing away from the gap. This phenomenon was not observed in Passian *et al.*'s experiment probably due to the small magnitude of the force within this range. A similar reverse in the force direction was reported in a study conducted by Aoki, *et al.* [23]. In their study, the Knudsen force on two noncoaxial circular cylinders with different temperatures was obtained via the numerical solution of the linearized Boltzmann equation with BGK collision model. It should be pointed out that the direction of the Knudsen force acting on the inner cylinder of Aoki *et al.*'s problem is the opposite of that in the present cantilever case. In addition, the reverse occurs near the continuum regime in their case as oppose to the near free-molecule regime in our case. To con-

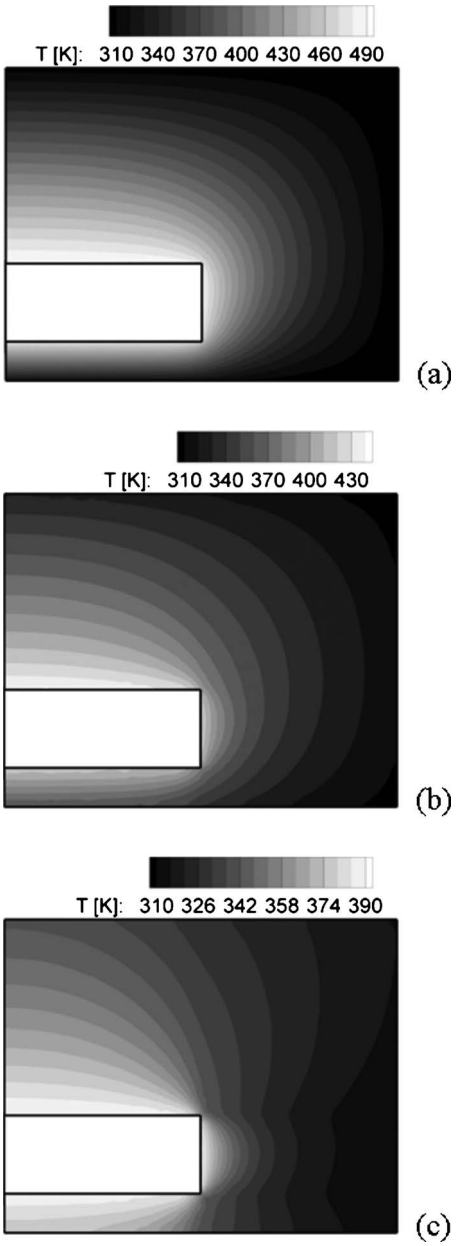

FIG. 2. Temperature contours for cases with 20×8 $\mu\mathrm{m}^2$ chamber and 10×2 $\mu\mathrm{m}^2$ beam: (a) Kn=0.056, (b) Kn=1.1, (c) Kn =56.

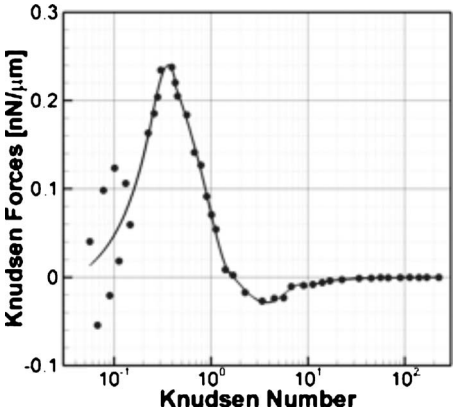

FIG. 3. Knudsen forces versus Knudsen numbers.

firm this finding, the developed DSMC code was employed to simulate Aoki *et al.*'s case and their results were reproduced. Further study illustrates that although the two systems are topologically similar, the shapes of structures play a critical role in the direction of the Knudsen force.

B. Flow structure and mechanism of the Knudsen force

Results shown in the previous section indicate that the Knudsen force is produced by the unbalanced gas pressure acting on the beam. The nonuniform pressure field constitutes a unique feature of rarefied gases in a nonuniform thermal environment. Unlike the continuum flows in which temperature inhomogeneity produces no macroscopic movement and no pressure gradients in the absence of external forces, bulk flows are induced in a rarefied gas under thermal loading. These flows drive gas molecules around and hence produce a nonuniform pressure distribution. A well-known example of this phenomenon is thermal transpiration which has been utilized as the primary driving force for Knudsen pumps [24,25].

The closely interrelated temperature and flow fields of a rarefied gas was recognized and investigated by Burnett and other investigators long time ago [26–28]. It was however not until late last century, systematical investigations were performed by Sone, Aoki, Ohwada *et al.* [23,29–33] using the asymptotic theory of Boltzmann equation, the DSMC method and experiments. Based on the asymptotic analysis of Boltzmann equation, several types of thermally induced flows were identified. Among them, thermal stress slip flow (TSS) which moves from the hot side to the cold side, is induced over a boundary along which the normal temperature gradient is nonuniform [31]. Thermal creep flow, on the other hand, is caused by the tangential temperature gradient near the wall and its direction is opposite to that of thermal stress slip flow. Thermal edge flow (TE) occurs when there are sharp configuration curvatures of the boundary [33]. The orders of these three types of flows are of second, first, 0.5th of Knudsen number, respectively. The mechanisms of these flows are ascribed to the anisotropy of momentum transfer onto the solid surface, which in turn produces a mechanical force acting on gas molecules and induces a bulk flow therein. Apart from the systematic studies by Sone and Aoki *et al.*, some thermal flows were also captured by Navier-Stokes solvers accompanied by the "Maxwell-Burnett" slip boundary condition [34] and deterministic solutions of ellipsoidal statistical (ES) kinetic model equation [18].

The Knudsen force is primarily caused by thermally driven flows. To fully understand its formation, flow structures must be carefully studied. Five representative flow fields of the model problem at Kn=0.11, Kn=0.37, Kn=1.1, Kn=2.3, and Kn=56 are plotted in Fig. 4. The corresponding Knudsen forces are positive in the first three cases, negative at Kn=2.3 and near zero at Kn=56.

In the continuum limit, i.e., $\mathrm{Kn}\to 0$, a nonuniform temperature field only produces a nonuniform density field. Pressure remains constant throughout the domain and no flow is induced. When the Knudsen number increases slightly from zero, four localized small vortices near the corners of the beam first appear as the result of thermal edge flows. Because of the small Knudsen number, the nonequilibrium regions are localized near the corners and the four vortices with one on the top surface, one on the bottom surface and two on the side of the beam are nearly symmetric about the neutral axis of the beam. Even though the local pressure near the corners increases due to the flows, they are about the same magnitude because of the symmetry and hence the net pressure along the vertical direction, i.e., the Knudsen force, is very weak. As the Knudsen number further increases to, for example, 0.11, the strength of thermal edge flows enhances which drive more gas molecules from the corners of the beam into the center of the beam and increase the pressure therein.

To provide a pictorial illustration of this phenomenon, consider a small area, ds, on the top surface of the beam near a corner as depicted in Fig. 5. Within a mean free path away from this area, molecules arrive to the surface without experiencing any intermolecular collision. Those molecules coming from point B have high temperatures while those from point A have low temperatures. As such, a net tangential momentum is impinged onto the surface when molecules collide with the beam. On the other hand, the reflected molecules have a symmetric distribution of their velocity distribution function due to diffuse walls. Hence a net tangential momentum is transferred to the wall and a force is exerted on gas molecules next to the wall which moves them from the corner into the center of the beam.

The high pressure near the surface of the beam promotes the formation of Poiseuille flows and hence vortices as shown in Fig. 4(a). On the top of the beam, the relatively spacious space allows a big vortex to be formed and the pressure driven flow effectively takes away some molecules from the top surface and thus releases some pressure therein. The bottom vortex is however constrained by the gap size and the Poiseuille flow cannot be formed effectively to move molecules away from the surface. In addition, the clockwise side vortex further blocks the gas molecules flowing out of the gap causing the pressure near the bottom surface of the beam to be higher than the pressure on the top surface of the beam. A sizable Knudsen force is thus produced. This force increases with the increased Knudsen number and reaches to its peak value near Kn=0.37. At this Knudsen number, the top vortex expands to its maximum strength and unites with

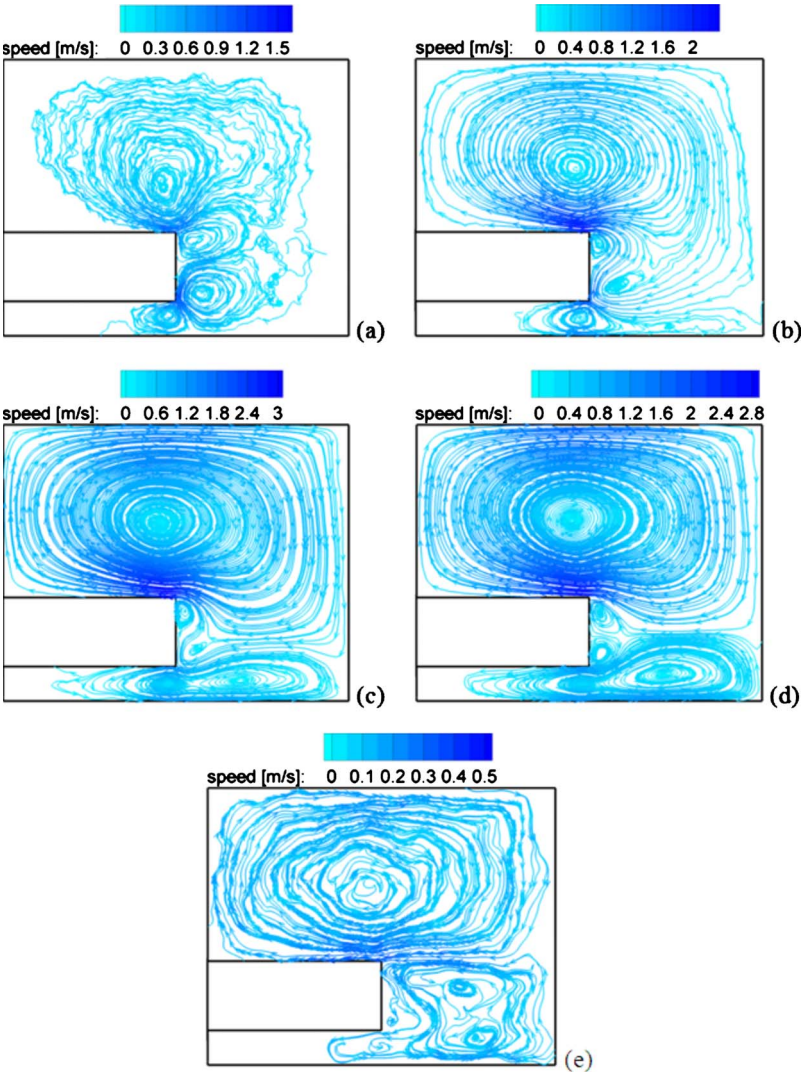

FIG. 4. (Color online) Flow structures throughout the domain (a) Kn=0.11, (b) Kn =0.37, (c) Kn=1.1, (d) Kn=2.3, (e) Kn=56.

the bottom side vortex to form a giant vortex as shown in Fig. 4(b). Those molecules near the top surface of the beam have been redistributed in the large space between the beam and the top wall of the enclosure. In the meantime, the size of the bottom vortex remains unchanged due to the constraints imposed by the gap size and the giant vortex. Hence the pressure difference between the top and the bottom surfaces of the beam reaches to its maximum value. As the Knudsen number further increases, gas becomes highly nonequilibrium and the mass flux near the bottom wall of the enclosure is no longer balanced. Molecules coming from the left side have a larger mass flux than that of molecules coming from the right side, i.e., the colder side. Such an imbalanced flux forms a flow next to the bottom wall going from the left to the right. This flow helps to take away molecules from the gap and forms a large counterclockwise vortex next to the bottom wall as shown in Fig. 4(c). The pressure next to the bottom beam is thus reduced and so is the Knudsen force. As the bottom vortex further expands laterally and gains its strength with the increased Knudsen number, the Knudsen force keeps decreasing and eventually reverses its direction as in the case at Kn=2.3 shown in Fig. 4(d). Near the free-molecule limit, i.e., Kn=56, the strengths of all thermally induced flows weaken [Fig. 4(e)] because the velocity density function at any point inside the domain becomes more isotropic. The pressure difference on the beam induced by these flows is reduced as well and in the free-molecule limit,

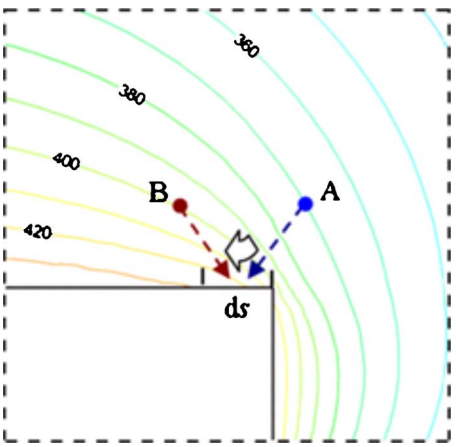

FIG. 5. (Color online) Schematic illustration of thermal edge flow (Contour lines and labels indicate the temperature distribution).

it goes to zero as expected from the gas kinetic theory.

Based on the above analysis, it is clear that thermal edge flows are the primary cause of the Knudsen force and the configuration of the problem domain plays a critical role in the flow generation and the formation of the Knudsen force particularly in the high Knudsen number regime. This in part explains the reverse force direction observed in Aoki *et al.*'s example. In their example, the Knudsen force is mainly caused by thermal stress slip flow and the asymmetric configuration.

IV. CONCLUSIONS

The Knudsen force acting on a structure with uniform temperature placed in a gaseous environment with nonuniform temperatures is numerically investigated over the entire flow regime using the DSMC method. The qualitative trend of the force as a function of the Knudsen number agrees very well with the experimental measurements conducted by Passian *et al.* and the maximum Knudsen force occurs in the transition regime. In the search for the origin of the Knudsen force, it has been found that thermally induced bulk flows are the main driven force for the creation of such a mechanical force. The configuration of the problem domain has a significant influence on the types of flows induced and hence on the magnitude as well as the direction of the force. In the model problem, i.e., a rectangular beam placed inside a rectangular enclosure, thermal edge flows are the main driving force, while in Aoki *et al.*'s problem, thermal stress slip flows are the main source at small Knudsen numbers. Such a finding indicates that for the beam type of structures such as the cantilever in the thermal sensing Atomic Force Microscope, one-dimensional model is not sufficient because of the significant effect of the corners and edges on the Knudsen force.

ACKNOWLEDGMENTS

This work is supported in part by Award No. SA-C0040/U.K.-C0016, made by King Abdullah University of Science and Technology, and in part by Hong Kong Research Grants Council under Competitive Earmarked Research Grant No. 621408.

[1] A. Passian *et al.*, J. Appl. Phys. **92**, 6326 (2002).
[2] A. Passian *et al.*, Ultramicroscopy **97**, 401 (2003); A. L. Lereu *et al.*, Appl. Phys. Lett. **84**, 1013 (2004).
[3] A. Passian, R. J. Warmack, T. L. Ferrell, and T. Thundat, Phys. Rev. Lett. **90**, 124503 (2003).
[4] B. Gotsmann and U. Durig, Appl. Phys. Lett. **87**, 194102 (2005).
[5] M. Scandurra, F. Iacopetti, and P. Colona, Phys. Rev. E **75**, 026308 (2007).
[6] N. Selden *et al.*, J. Fluid Mech. **634**, 419 (2009); N. Selden, C. Ngalande, S. Gimelshein, E. P. Muntz, A. Alexeenko, and A. Ketsdever, Phys. Rev. E **79**, 041201 (2009).
[7] W. Crooks, Philos. Trans. R. Soc. London **163**, 277 (1873); **165**, 519 (1875).
[8] O. Reynolds, Philos. Trans. R. Soc. London **166**, 725 (1876); **170**, 727 (1879).
[9] J. C. Maxwell, Philos. Trans. R. Soc. London **170**, 231 (1879).
[10] M. Knudsen, *The Kinetic Theory of Gases* (Methuen & Co. LTD, London, 1934).
[11] A. Einstein, Z. Phys. **27**, 1 (1924).
[12] L. Carbone, A. Cavalleri, G. Ciani, R. Dolesi, M. Hueller, D. Tombolato, S. Vitale, and W. J. Weber, Phys. Rev. D **76**, 102003 (2007).
[13] M. Ota, T. Nakao, and M. Sakamoto, Math. Comput. Simul. **55**, 223 (2001).
[14] D. C. Wadsworth and E. P. Muntz, J. Microelectromech. Syst. **5**, 59 (1996).
[15] G. Benford and J. Benford, Acta Astronaut. **56**, 529 (2005).
[16] D. Jones, Nature (London) **392**, 337 (1998); **392**, 443 (1998); **395**, 120 (1998).
[17] E. Brüche and W. Littwin, Z. Phys. **52**, 318 (1929).
[18] A. A. Alexeenko and E. P. Muntz, *Collection of Technical Papers—36th AIAA Fluid Dynamics Conference* (American Institute of Aeronautics and Astronautics, Reston, VA, 2006), Vol. 3, p. 1907.
[19] G. A. Bird, *Molecular Gas Dynamics and the Direct Simulation of Gas Flows* (Clarendon Press, Oxford, 1994).
[20] C. Cercignani, *The Boltzmann Equation and Its Applications* (Springer-Verlag, New York, 1988).
[21] G. Karniadakis, A. Beskok, and N. Aluru, *Microflows and Nanoflows: Fundamentals and Simulation* (Springer, New York, 2005).
[22] E. P. Muntz, Annu. Rev. Fluid Mech. **21**, 387 (1989); E. S. Oran, C. K. Oh, and B. Z. Cybyk, *ibid.* **30**, 403 (1998).
[23] K. Aoki, Y. Sone, and T. Yano, Phys. Fluids A **1**, 409 (1989).
[24] S. McNamara and Y. B. Gianchandani, J. Microelectromech. Syst. **14**, 741 (2005).
[25] E. P. Muntz and S. E. Vargo, in *The MEMS Handbook*, edited by M. Gad-el-Hak (CRC, Boca Raton, Florida, 2002).
[26] D. Burnett, Proc. London Math. Soc. **s2-39**, 385 (1935).
[27] S. Chapman and T. G. Cowling, *The Mathematical Theory of Non-Uniform Gases* (Cambridge University Press, New York, 1990).
[28] M. N. Kogan, Annu. Rev. Fluid Mech. **5**, 383 (1973).
[29] K. Aoki, Y. Sone, and Y. Waniguchi, Comput. Math. Appl. **35**, 15 (1998).
[30] Y. Sone, Annu. Rev. Fluid Mech. **32**, 779 (2000); *Molecular Gas Dynamics, Theory, Techniques, and Applications* (Birkhuser, Boston, 2007).
[31] Y. Sone, Phys. Fluids **15**, 1418 (1972); T. Ohwada and Y. Sone, Eur. J. Mech. B/Fluids **11**, 389 (1992).
[32] Y. Sone, S. Takata, and H. Sugimoto, Phys. Fluids **8**, 3403 (1996).
[33] K. Aoki, Y. Sone, and N. Misukawa, in *Proceedings of the 19th International Symposium on Rarefied Gas Dynamics* (Oxford University Press, London, 1995); Y. Sone and M. Yoshimoto, Phys. Fluids **9**, 3530 (1997).
[34] D. A. Lockerby, J. M. Reese, D. R. Emerson, and R. W. Barber, Phys. Rev. E **70**, 017303 (2004).